CONF-771052-3

EFFECT OF SODIUM ENVIRONMENT ON THE CREEP-RUPTURE AND LOW-CYCLE FATIGUE BEHAVIOR OF AUSTENITIC STAINLESS STEELS*

K. Natesan, O. K. Chopra, G. J. Zeman,
D. L. Smith, and T. F. Kassner

Materials Science Division
ARGONNE NATIONAL LABORATORY

September 1977

EFFECT OF SODIUM ENVIRONMENT ON THE CREEP-RUPTURE AND LOW-CYCLE FATIGUE BEHAVIOR OF AUSTENITIC STAINLESS STEELS*

K. Natesan, O. K. Chopra, G. J. Zeman, D. L. Smith, and T. F. Kassner

Materials Science Division
ARGONNE NATIONAL LABORATORY
Argonne, Illinois 60439

September 1977

To be presented at the *IAEA/IWGFR Specialists Meeting on "Properties of Primary Circuit Structural Materials Including Environmental Effects,"* October 17-21, 1977, INTERATOM, Bensberg, Federal Republic of Germany.

*Work supported by the U. S. Energy Research and Development Administration.

EFFECT OF SODIUM ENVIRONMENT ON THE CREEP-RUPTURE AND LOW-CYCLE FATIGUE BEHAVIOR OF AUSTENITIC STAINLESS STEELS*

K. Natesan, O. K. Chopra, G. J. Zeman, D. L. Smith, and T. F. Kassner

Materials Science Division
ARGONNE NATIONAL LABORATORY
Argonne, Illinois 60439

ABSTRACT

Austenitic stainless steels used for in-core structural components, piping, valves, and the intermediate heat exchanger in Liquid-Metal Fast-Breeder Reactors (LMFBRs) are subjected to sodium at elevated temperatures and to complex stress conditions. As a result, the materials can undergo compositional and microstructural changes as well as mechanical deformation by creep and cyclic fatigue processes. In the present paper, information is presented on the creep-rupture and low-cycle fatigue behavior of Types 304 and 316 stainless steel in the solution-annealed condition and after long-term exposure to flowing sodium. The nonmetallic impurity-element concentrations in the sodium were controlled at levels similar to those in EBR-II primary sodium. Strain-time relationships developed from the experimental creep data were used to generate isochronous stress-creep strain curves as functions of sodium-exposure time and temperature. The low-cycle fatigue data were used to obtain relationships between plastic strain range and cycles-to-failure based on the Coffin-Manson formalism and a damage-rate approach developed at ANL. An analysis of the cyclic stress-strain behavior of the materials showed that the strain-hardening rates for the sodium-exposed steels were larger than those for the annealed material. However, the sodium-exposed specimens showed significant softening, as evidenced by the lower stress at half the fatigue life. Microstructural information obtained from the different specimens suggests that crack initiation is more difficult in the long-term sodium-exposed specimens when compared with the solution-annealed material. Based on the expected carbon concentrations in LMFBR primary system sodium, moderate carburization of the austenitic stainless steels will not degrade the mechanical properties to a significant extent, and therefore, will not limit the performance of out-of-core components.

---

*Work supported by the U. S. Energy Research and Development Administration.

EFFECT OF SODIUM ENVIRONMENT ON THE CREEP-RUPTURE AND LOW-CYCLE FATIGUE BEHAVIOR OF AUSTENITIC STAINLESS STEELS*

K. Natesan, O. K. Chopra, G. J. Zeman, D. L. Smith, and T. F. Kassner

Materials Science Division
ARGONNE NATIONAL LABORATORY
Argonne, Illinois 60439

INTRODUCTION

The austenitic stainless steels used for in-core structural components, piping, valves, and the intermediate heat exchanger in Liquid-Metal Fast-Breeder Reactors (LMFBRs) are subjected to sodium at elevated temperatures and to complex stress conditions. In the case of out-of-core components that have a design life of 20 to 30 y, large extrapolations of mechanical-property data, obtained in air or inert-gas environments over relatively short periods, are required. Furthermore, the influence of the time- and temperature-dependent migration of carbon and nitrogen in the materials that results from exposure to flowing sodium must be considered.[1]

Nonmetallic elements such as carbon and nitrogen mitrate in sodium heat-transport systems as a result of chemical activity differences. The conditions of temperature and carbon concentration in sodium that result in either carburization or decarburization of Types 304L and 316 stainless steel (with nominal initial carbon contents) are shown in Fig. 1.[2] The results indicate that Type 316 stainless steel would not carburize at temperatures below ∿640°C in the Experimental Breeder Reactor (EBR-II) sodium, whereas the carburization-decarburization crossover temperature in the Fast Flux Test Facility (FFTF) would be ∿560 and 510°C for core outlet temperatures of 566 and 474°C, respectively. Furthermore, it has also been shown that the anticipated carbon levels in the FFTF primary sodium circuit are ∿0.025 and 0.065 ppm for core outlet temperatures of 474 and 566°C, respectively. The extent to which the steels undergo carburization depends on the sodium-exposure time, temperature, and thermal-mechanical history of the material that influences its microstructure. A mathematical analysis has been developed[3] to obtain carbon concentration-distance profiles as functions of time, temperature, and carbon concentration

*Work supported by the U. S. Energy Research and Development Administration.

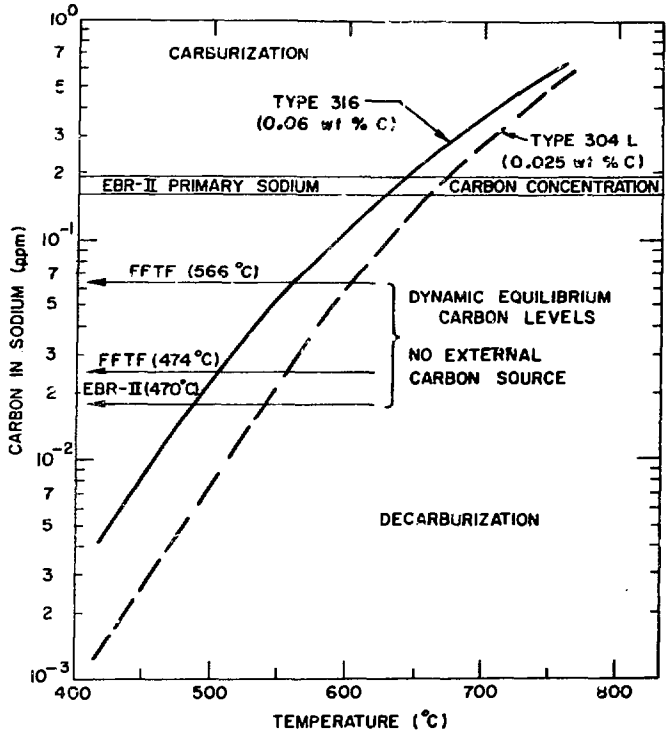

Fig. 1. Carburization-Decarburization Regimes for Types 316 and 304L Stainless Steels in the FFTF and EBR-II Primary Sodium Systems, Respectively, in Terms of the Carbon Concentration in Sodium and Temperature.

in sodium. Because of the relatively low operating temperatures and large section thicknesses in structural components, carbon concentration profiles rather than a uniform equilibrium carbon distribution will result in the materials during reactor service. Thus, it is essential to obtain mechanical-property data on materials with specific carbon penetration depths and to correlate the property changes with carbon concentration in sodium as well as exposure time and temperature.

In the present paper, data are presented on the effect of carburization on the creep rupture and low-cycle fatigue behavior of Types 304 and 316 stainless steel in the temperature range of 550 to 700°C. A carbon concentration in sodium of ∿0.4 ppm was maintained during the exposure of mechanical test specimens. This carbon concentration value is approximately a factor of two larger than that in EBR-II primary circuit sodium and it is believed to be an upper bound value for a large LMFBR system.

EXPERIMENTAL PROCEDURE

Types 304 and 316 stainless steel, that are used extensively in breeder-reactor research programs in the USA, were procured in flat and bar stock and cold rolled to sheet and rod form suitable for fabrication of mechanical test specimens. The composition of the steels is given in Table I. The creep test specimens were solution annealed for 1800 s in argon at 1025°C and water quenched. The annealed specimens of Types 304 and 316 stainless steel had grain sizes of ∿25 and 15 μm, respectively. Uniaxial creep specimens, designed and fabricated in accordance with ASTM Standard E8-69, had a gauge length of 22.2 mm, width of 5.59 mm, and thickness of 0.375 mm. The low-cycle fatigue specimens had a gauge length of 12.7 mm and a gauge diameter of 5.08 mm.

TABLE I. Composition of Austenitic Stainless Steels

Type 304 (Heat 9T2796)		Type 316 (Heat V87210)	
Element	Concentration, wt %	Element	Concentration, wt %
C	0.046	C	0.058
N	0.038	N	0.007
P	0.026	P	0.026
S	0.012	S	0.011
Cr	17.7	Cr	16.7
Ni	9.3	Ni	13.9
Mn	1.17	Mn	1.43
Si	0.47	Si	0.46
Mo	0.33	Mo	2.84
Ti	0.03	Ti	0.04
Cu	0.20	Cu	0.06
Co	0.10	Co	0.03

The fatigue samples were solution annealed at 1050°C for 1800 s in argon and water quenched. The grain sizes of the annealed specimens were 65 and 45 μm for Types 304 and 316 stainless steel, respectively. The creep tests were conducted on conventional constant-load creep-rupture machines in an argon environment at temperatures between 550 and 700°C over a stress range of 55 to 350 MPa. The creep strain in the specimens was measured by a linear-variable-differential transducer, in which displacements of 5 μm could be accurately

determined. The low-cycle fatigue tests were conducted in a 9000 kg MTS closed-loop servo-controlled hydraulically-actuated fatigue machine equipped with a sodium loop. The specimen stress was determined by a fatigue-rated load cell attached to the actuator. Since direct measurement of the specimen strain in the sodium environment was not considered feasible, the tests were conducted in a stroke-control mode by means of a standard resistive-type extensometer located on the upper portion of the fixture in an ambient temperature region. The tests were conducted at strain rates of $\sim 4 \times 10^{-3}$ and 4×10^{-5} s^{-1} with a fully-reversed triangular waveform and a zero mean strain. Additional details of the specimen geometry, test equipment, and procedures for strain calculations were reported earlier [4]

The sodium facility that was used for the exposure of mechanical test specimens has also been described.[5] The oxygen concentration in sodium was <1 ppm for all experiments. The carbon concentration in sodium was determined by equilibrating a high-purity Fe-18 wt % Cr-8 wt % Ni alloy in sodium and using the reported[6] data on the distribution of carbon between this alloy and sodium. The carbon concentration in sodium was $\sim$0.4 ppm for all experiments. Mechanical test specimens were exposed to flowing sodium at temperatures of 550, 600, 650, and 700°C for times between 0.43 and 18.04 Ms to produce carbon penetration depths of $\sim$0.10, 0.20, and 0.375 mm, which were calculated from the mathematical analysis in Ref. 3. The specimens were subsequently used in creep-rupture tests in an argon environment or in low-cycle fatigue tests in a flowing sodium system.

RESULTS AND DISCUSSION

Creep-rupture Results

Figures 2 and 3 show the variations in rupture life and minimum creep rate with applied stress for Types 304 and 316 stainless steel specimens in both the annealed and sodium-exposed conditions at temperatures between 550 and 700°C. The surface carbon concentrations in the mechanical test specimens were determined from combustion analyses of 50-μm-thick foils of the same material equilibrated in sodium during the specimen-exposure period. The values obtained for Type 304 stainless steel were $\sim$0.05 wt % at 700°C, 0.25 wt % at 650°C, and 0.30 wt % at 600°C. The average carbon concentrations in the sodium-exposed specimens ranged from 0.043 to 0.046 wt % at 700°C, 0.078 to 0.195 wt % at 650°C, and 0.145 to 0.25 wt % at 600°C; the larger values at each temperature

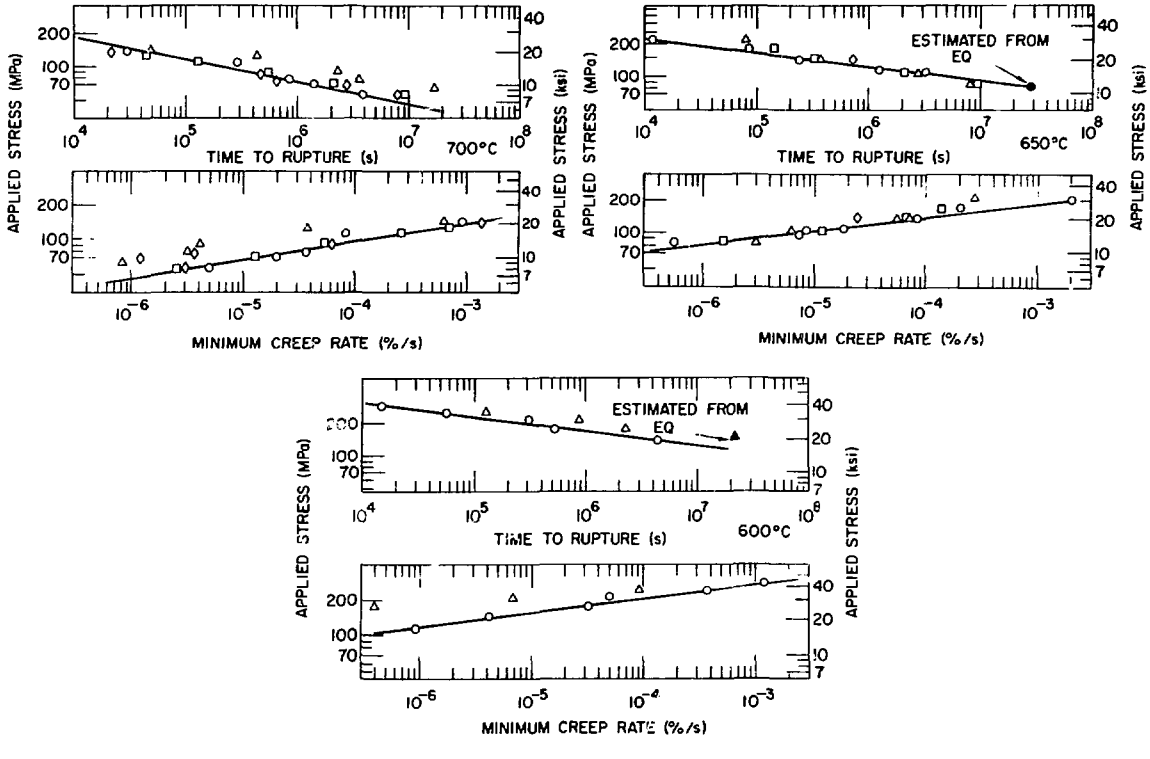

Fig. 2. Variation of Time to Rupture and Minimum Creep Rate with Applied Stress for Type 304 Stainless Steel at 700, 650, and 600°C. Solution annealed: O, carburization depths: △ = 100 μm, □ = 200 μm, and ◇ = 375 μm.

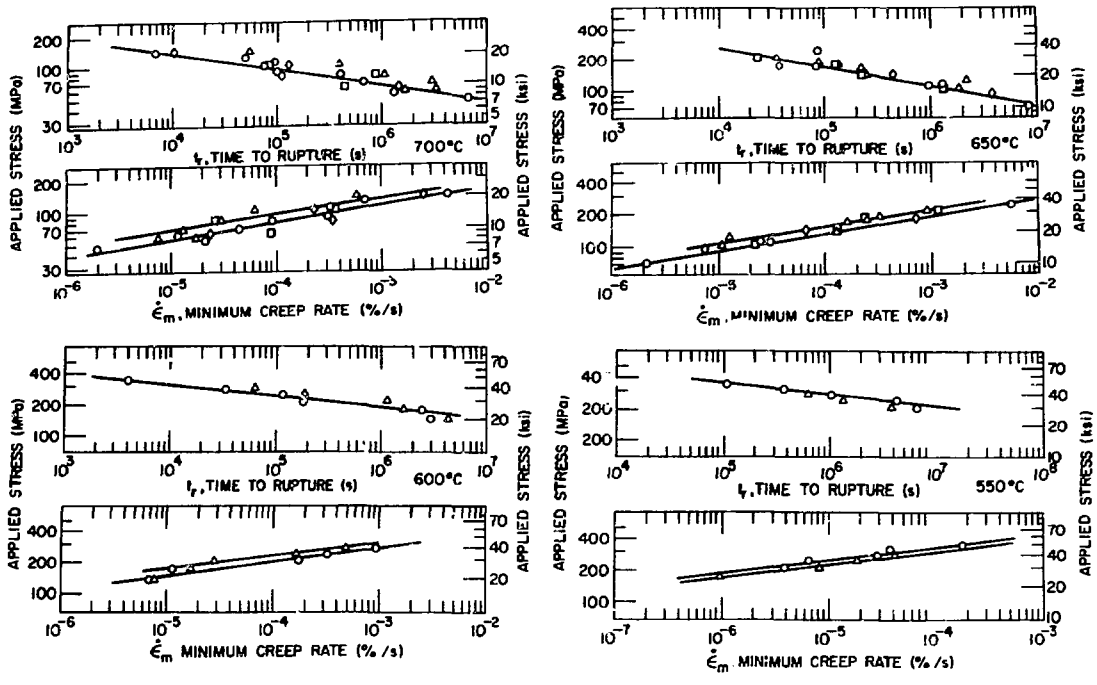

Fig. 3. Variation of Time to Rupture and Minimum Creep Rate with Applied Stress for Type 316 Stainless Steel at 700, 650, 600, and 550°C. Solution annealed: O, carburization depths: △ = 100 μm, □ = 200 μm, and ◇ = 375 μm.

result from longer exposure times. The surface concentration values obtained for Type 316 stainless steel were 0.16 wt % at 700°C, 0.34 wt % at 650°C, 0.52 wt % at 600°C, and 0.65 wt % at 550°C. The corresponding average carbon concentrations in the sodium-exposed specimens were 0.259 wt % at 550°C (after 18.04 Ms exposure), 0.153 wt % at 600°C (after 5.44 Ms exposure) and ranged from 0.085 to 0.145 wt % at 650°C, and 0.063 to 0.075 wt % at 700°C for exposure times up to 18.04 and 5.44 Ms, respectively. In general, the creep data show that for the range of carburization attained by exposure of the stainless steels to the sodium, the rupture life increases and the minimum creep rate decreases (except in the case of Type 316 stainless steel exposed at 550°C) when compared with the results for the materials in the solution-annealed condition. Detailed analyses of creep strain-time curves for various specimens showed that at any given test temperature the observed fracture strain was independent of the sodium-exposure time and that the strain accumulated during the second stage of creep decreased with a decrease in applied stress. At temperatures between 550 and 700°C, the strain at rupture ranged from 30 to 70%, respectively, for specimens in both the solution-annealed and sodium-exposed

conditions. The strains accumulated in the specimens in the first and second stages of creep were between 2 and 10 and 15 and 30%, respectively, of the fracture strain, where the larger values correspond to the lowest test temperature.

Microstructural Observations

A comparison of the microstructures of the sodium-exposed specimens (in the axial direction) before and after testing showed that creep deformation resulted in elongated grains in specimens which exhibited large rupture strains. In specimens of Type 304 stainless steel, the carbide particles precipitate preferentially at the grain boundaries and the size of the particles increases as the sodium-exposure time increases. The carbide particles in Type 316 stainless steel were observed both in grain boundaries and in the interior of the grains; furthermore, for long exposure times, the Type 316 stainless steel specimens also contained Fe_2Mo intermetallic phase. The fracture surfaces of the annealed and sodium-exposed specimens creep tested at different stress levels were dimpled,[7] which is indicative of a ductile failure mode that is associated with the growth of internal voids or holes. Scanning-electron micrographs of the fracture surfaces of the solution-annealed and sodium-exposed specimens of Type 304 stainless steel[8] tested at various strain rates are shown in Figs. 4 and 5 for test temperatures of 600 and 700°C, respectively. These micrographs indicate a transition in the fracture mode from a completely dimpled structure to a partially intergranular fracture as the strain rate decreases. The transition occurs at a higher strain rate at the lower temperatures. For example, in the solution-annealed specimens tested at 600°C, the fracture surface shows a completely dimpled structure at a strain rate of 3.81×10^{-4} s^{-1} (Fig. 4a), whereas evidence of intergranular fracture on some of the surfaces is apparent at a strain rate of 3.81×10^{-5} s^{-1} (Fig. 4b). At a creep rate of 2×10^{-7} s^{-1}, the fracture is mostly intergranular. A similar transition in the fracture mode occurs in the solution-annealed specimens at 700°C although the specimens that failed in a ductile manner exhibited large cavities and voids rather than a dimpled structure. Sodium exposure tends to inhibit the intergranular failure mode observed at the lower strain rates; i.e., the extent of intergranular fracture in Fig. 4f for the sodium-exposed specimens is considerably less than that in the solution-annealed material (Fig. 4c) at the lowest strain rate.

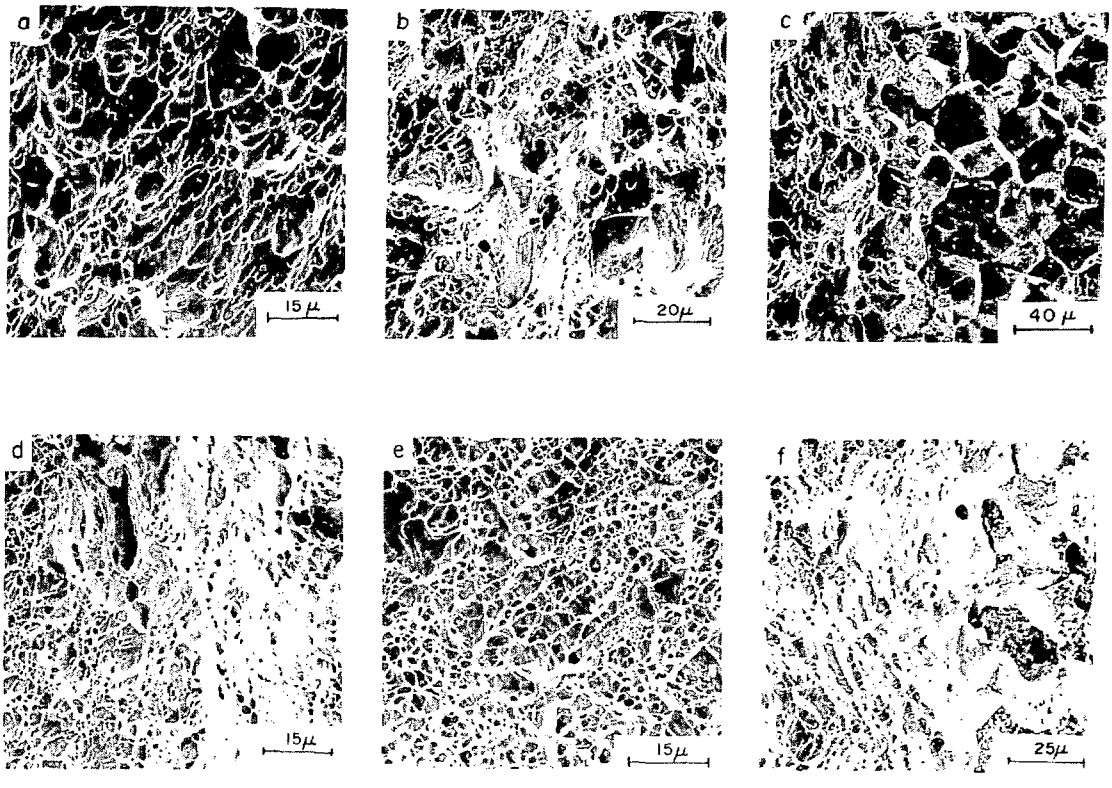

Fig. 4. Scanning-electron Micrographs of Fracture Surfaces of Type 304 Stainless Steel Tested at 600°C. (a)-(c) solution-annealed condition and (d)-(f) exposed to sodium for 18.04 Ms at 600°C. (a) and (d) $\dot{\varepsilon} = 3.81 \times 10^{-4}\ s^{-1}$, (b) and (e) $\dot{\varepsilon} = 3.81 \times 10^{-5}\ s^{-1}$, (c) $\dot{\varepsilon} = 2.0 \times 10^{-7}\ s^{-1}$, and (f) $\dot{\varepsilon} = 4.1 \times 10^{-8}\ s^{-1}$.

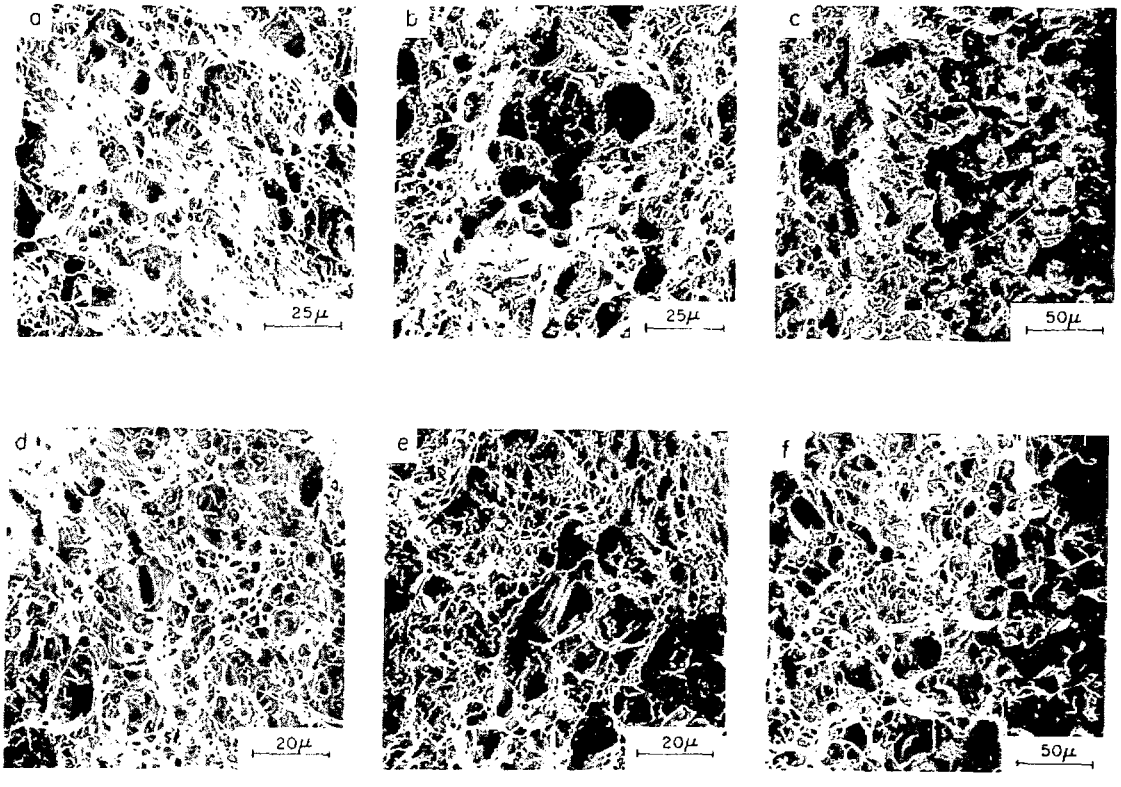

Fig. 5. Scanning-electron Micrographs of Fracture Surfaces of Type 304 Stainless Steel Tested at 700°C. (a)-(c) solution-annealed condition and (d)-(f) exposed to sodium for 5.44 Ms at 700°C. (a) and (d) $\dot{\varepsilon} = 3.81 \times 10^{-4}\ s^{-1}$, (b) and (e) $\dot{\varepsilon} = 3.81 \times 10^{-5}\ s^{-1}$, (c) $\dot{\varepsilon} = 8.3 \times 10^{-7}\ s^{-1}$, and (f) $\dot{\varepsilon} = 6.95 \times 10^{-6}\ s^{-1}$.

Creep-rupture Correlations

To understand creep-rupture behavior more fully, correlations between rupture life and other parameters were determined from the creep curves.[9] Current elevated-temperature design rules[10] require not only a knowledge of rupture behavior, but also information on the time to the onset of tertiary creep and time to accumulate a specified strain. Tertiary creep is generally indicative of material cracking and void formation, and therefore, it is metallurgically related to material damage. Also, tertiary creep results in material instability at high values of strain, since the strain rate increases as the creep-induced strain becomes more concentrated. As a result, a correlation between the rupture life t_r and the time-to-tertiary creep t_2 can be used to establish

the onset of instability in component design evaluations. The correlations that were developed between various creep parameters for Types 304 and 316 stainless steel are listed in Table II.

The time to a specified strain limit (currently set at 1% total inelastic membrane strain) can be determined from isochronous stress-strain curves.[11] The experimental strain-time curves were analyzed in terms of the creep equation developed by Booker[12]

$$\varepsilon = \frac{dpt}{1 + pt} + \dot{\varepsilon}_m t \ , \qquad (1)$$

where ε is the creep strain, d the intercept strain, $\dot{\varepsilon}_m$ the minimum creep rate, and t the time. The parameter p is related to the curvature of the primary portion of the curve. Analytical expressions given in Table II were used in Eq. (1) to compute the strain-time curves and to subsequently generate the isochronous stress-strain plots for Types 304 and 316 stainless steel, which are shown in Figs. 6 and 7. The results indicate that the carburization of the steel in the sodium environment in the range of our investigation enhances the creep-rupture properties of the materials (except for Type 316 stainless steel at 550°C). Additional experiments are being conducted on Type 316 stainless steel at temperatures $\leq$550°C to evaluate the cause(s) for the degradation in creep properties of this material upon exposure to a sodium environment.

Low-cycle Fatigue Results

Low-cycle fatigue data have been obtained on Types 304 and 316 stainless steel in solution-annealed, thermally aged, and sodium-exposed conditions. Values for the total strain range $\Delta\varepsilon_t$, plastic strain range $\Delta\varepsilon_p$, cyclic stress range at half the fatigue life $\Delta\sigma_{\frac{1}{2}N_f}$, fatigue life N_f, and time to failure t_f have been reported earlier for the two materials under a variety of sodium-exposure and test conditions.[13,14] Figure 8 shows the relationship between plastic strain range and the fatigue life for Type 304 stainless steel in solution-annealed and thermally aged conditions and after 5.44 and 18.04 Ms exposures to sodium at 600°C. The results show (Fig. 8a) that the fatigue life of the thermally aged material is significantly larger than that of the annealed material, especially for $\Delta\varepsilon_p$ <0.6%. A decrease in strain rate lowers the fatigue life of the aged material and increases the life of the annealed material.

TABLE II. Creep Correlations for Types 304 and 316 Stainless Steel

$$t_r(s) = C\,[\dot{\varepsilon}_m\ (\%/s)]^{-\alpha} \qquad (2)$$

Treatment	304 SS α	304 SS c	316 SS α	316 SS c
Solution Annealed	0.99	24.05		
Na Exposed at 650 and 700°C	0.95	33.81		
Na Exposed at 600°C	0.79	99.93		
All Data (550 to 700°C)	-	-	0.986	33.6

$$t_2(s) = B\,[t_r(s)]^{\beta} \qquad (3)$$

Treatment	304 SS β	304 SS B	316 SS β	316 SS B
Solution Annealed	1.025	0.455		
Na Exposed (All Temperatures)	1.061	0.288		
All Data	1.05	0.333	1.033	0.327

$$\dot{\varepsilon}_2\ (\%/s) = D\,[\dot{\varepsilon}_m\ (\%/s)]^{\gamma} \qquad (4)^a$$

Treatment	304 SS γ	304 SS D	316 SS γ	316 SS D
Solution Annealed	0.987	0.964		
Na Exposed at 650 and 700°C	0.972	0.858		
Na Exposed at 600°C	0.918	0.549		
All Data (550 to 700°C)			1.002	1.016

$$\dot{\varepsilon}_m\ (\%/s) = A\,[\sigma\ (MPa)]^{n} \qquad (5)$$

Treatment	Temperature (°C)	304 SS n	304 SS A	316 SS n	316 SS A
Solution Annealed	700	5.60	8.23×10^{-16}	6.38	8.7×10^{-17}
Solution Annealed	650	5.90	1.60×10^{-17}	6.53	1.6×10^{-18}
Solution Annealed	600	6.40	8.34×10^{-20}	7.35	1.12×10^{-21}
Solution Annealed	550			7.87	1.43×10^{-24}
Sodium Exposed	700	6.23	4.35×15^{-17}	7.27	4.3×10^{-19}
Sodium Exposed	650	6.48	5.14×10^{-19}	6.42	1.0×10^{-18}
Sodium Exposed	600	10.71	2.48×10^{-30}	8.10	7.0×10^{-24}
Sodium Exposed	550			8.23	5.2×10^{-25}

[a] In Eq. (4), $\dot{\varepsilon}_2$ is the ratio of the strain-to-time at the onset of third stage creep.

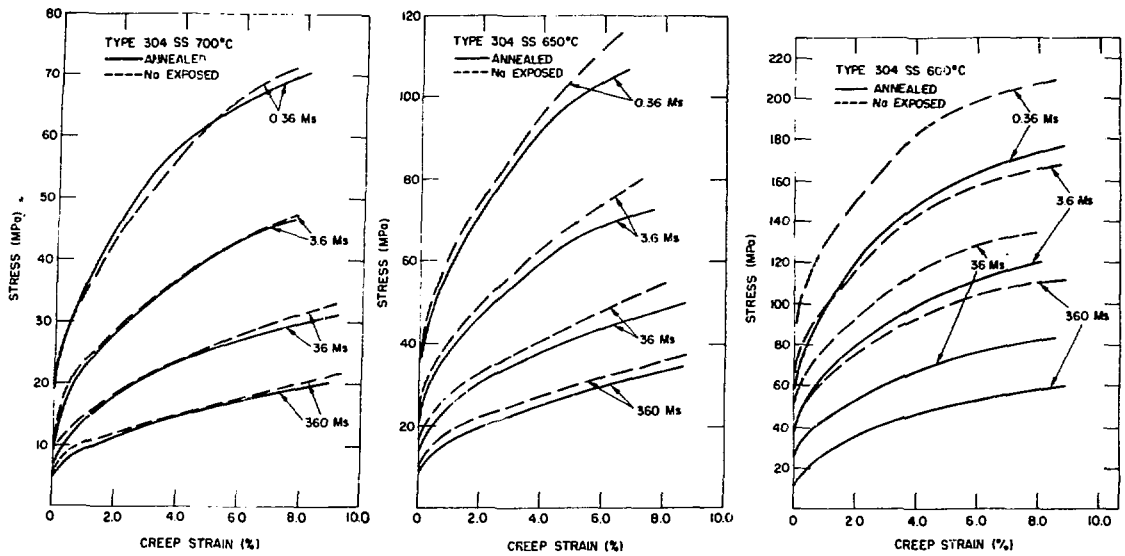

Fig. 6. Isochronous Stress-creep Strain Curves for Type 304 Stainless Steel in Solution-annealed and Sodium-exposed Conditions.

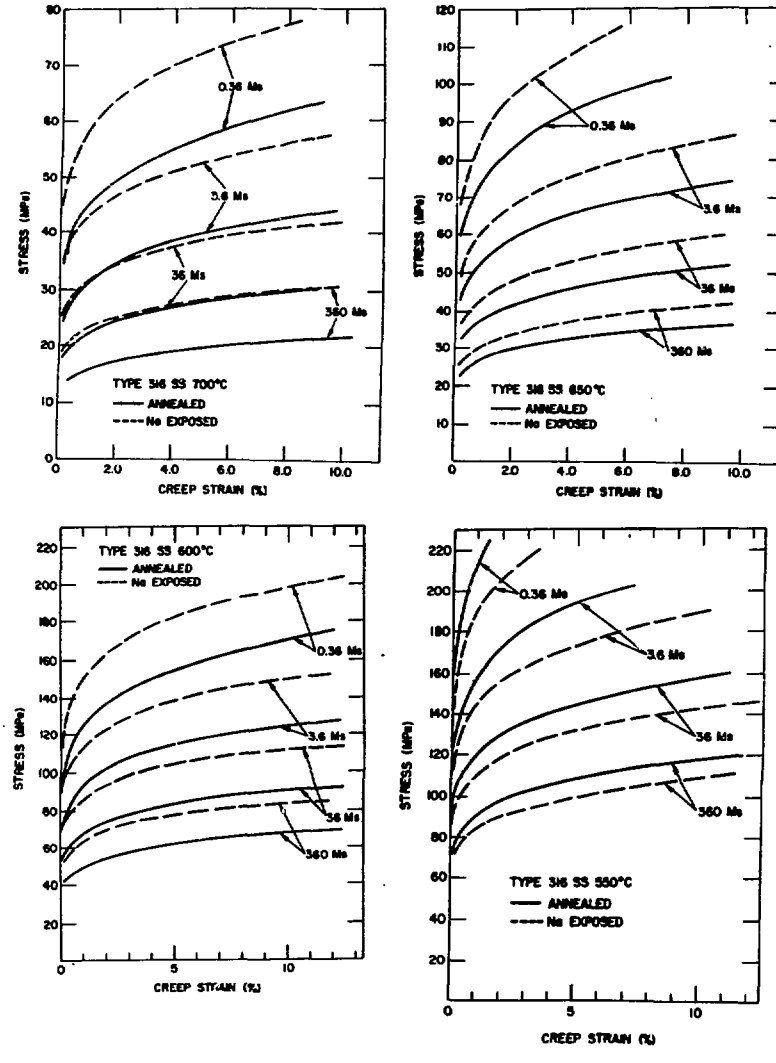

Fig. 7. Isochronous Stress-creep Strain Curves for Type 316 Stainless Steel in Solution-annealed and Sodium-exposed Conditions.

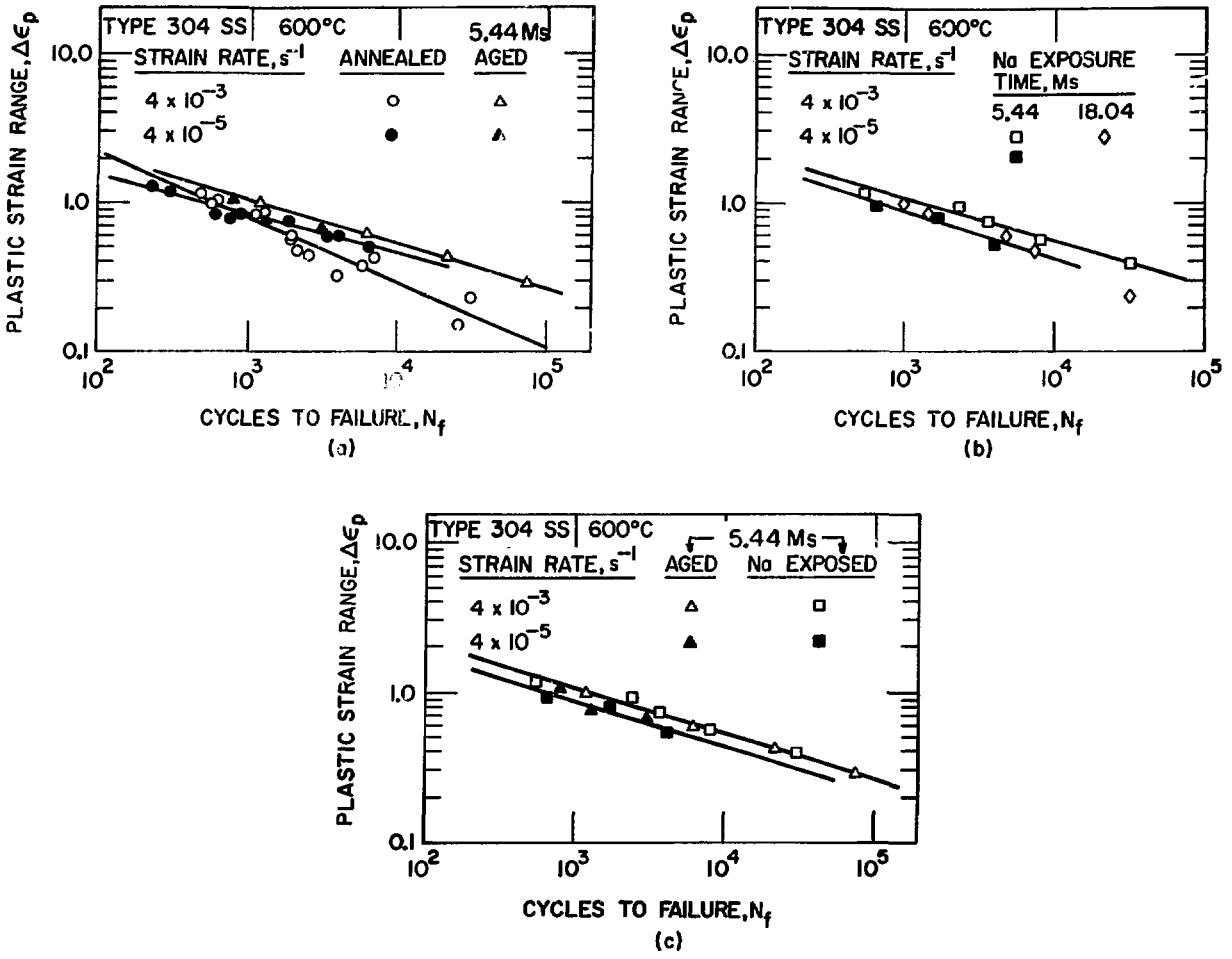

Fig. 8. Fatigue Data Obtained on Type 304 Stainless Steel in the Annealed, Aged, and Sodium-exposed Conditions at 600°C. The carbon penetration depths for the 5.44 and 18.04 Ms exposure times were ∿100 and 200 μm, respectively.

The latter effect results from in-situ aging of the material during the testing period; aging is probably enhanced by the applied stress on the specimens. Therefore, one must consider differences between the behavior of aged and sodium-exposed materials in order to quantitatively evaluate the influence of long-term sodium exposure on the fatigue properties of the materials. Figure 8c shows a comparison of the fatigue life of aged and sodium-exposed materials at strain rates of ∿4 x 10^{-3} and 4 x 10^{-5} s^{-1}. The figure clearly shows that carburization of the specimens in the range of our investigation at 600°C has negligible effect on the fatigue life of the material. Furthermore, the results show that a decrease in strain rate by two orders of magnitude lowers the cycles to failure by a factor of two at 600°C.

Figure 9 shows the relationship between plastic strain range and fatigue life for Type 304 stainless steel at 550 and 700°C. The data at 550°C show that the fatigue life of the aged material is a factor two greater than that of the annealed specimens. The results also show that very little in-situ aging occurs in the solution-annealed material at 550°C even for the comparatively long test time associated with a $\Delta\varepsilon_p$ = 0.3%. The fatigue life of the sodium-exposed specimens is significantly smaller than that of the aged material. This difference can only be attributed to carburization of the sodium-exposed specimens since the exposure time at 550°C was 18.04 Ms for both types of specimens. The surface carbon content in the sodium-exposed specimens was 0.8 wt % and the depth of carbon penetration was 150 to 200 μm.

The data at 700°C indicate that the aged specimens have a longer fatigue life than the sodium-exposed material. The carbon concentration in sodium resulted in slight decarburization of the Type 304 stainless steel, which had an initial carbon content of 0.046 wt %. Thus, the decrease in the fatigue life of the sodium-exposed specimens can be attributed to carbon loss from ∿375-μm-thick region of the specimens.

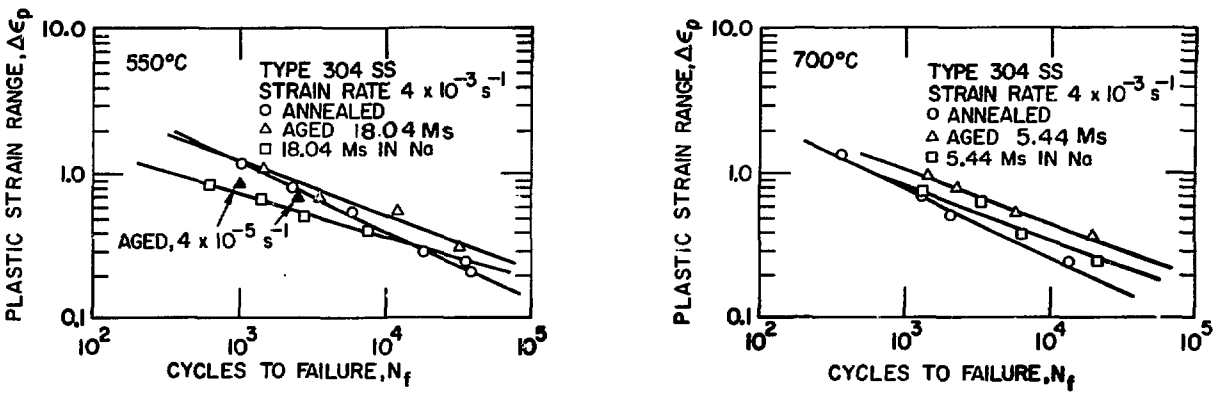

Fig. 9. Fatigue Data Obtained on Type 304 Stainless Steel in the Annealed, Aged, and Sodium-exposed Conditions at 550 and 700°C. The carbon penetration depth was ∿100 μm for the sodium-exposed specimens at 550°C. At 700°C, slight decarburization of the specimens occurred to a depth of ∿375 μm.

Figure 10 shows the relationship between the plastic strain range and fatigue life for Type 316 stainless steel specimens in the solution-annealed, aged, and sodium-exposed conditions at temperatures of 550, 600, and 700°C. The data at 600°C show that at a given plastic strain range, the fatigue life of specimens in the aged condition and after 5.44 and 18.04 Ms exposure to sodium is similar, and the life is somewhat greater than that of the annealed material. The data at 600°C indicate that the combined effects of thermal aging and carburization in sodium on the fatigue life are minimal when compared with behavior of solution-annealed Type 316 stainless steel. Additional data on thermally aged material at 550 and 700°C are required to assess the effect of long-term sodium exposure on the fatigue properties.

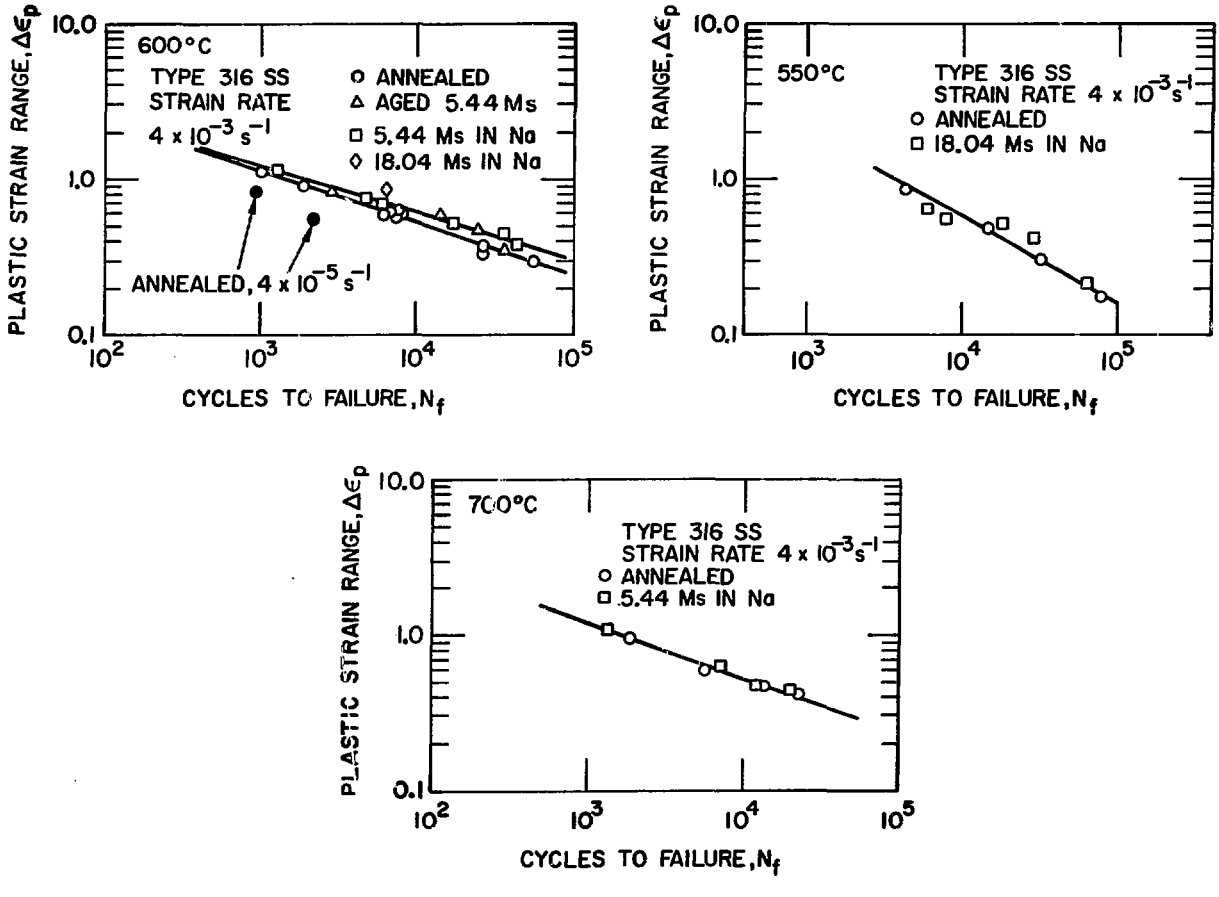

Fig. 10. Fatigue Data Obtained on Type 316 Stainless Steel in the Annealed, Aged, and Sodium-exposed Conditions at Temperatures of 550, 600, and 700°C. The carbon penetration depths at 600°C for the 5.44 and 18.04 Ms sodium-exposure times were ∿100 and 200 μm, respectively. The penetration depths for the exposed specimens at 550 and 700°C were ∿100 and 375 μm, respectively.

Analysis of Cyclic Stress-Fatigue Life Behavior

To understand the effect of metallurgical history on the mechanical behavior under fatigue loading conditions, hysteresis loops from different tests were analyzed and plots of cyclic stress as a function of the number of cycles were generated for specimens that have undergone different treatments. Figure 11 shows the cyclic stress versus fatigue cycles (at a total strain range $\Delta\varepsilon_t$ = 1.0%) for Type 304 stainless steel at 550, 600, and 700°C and for Type 316 stainless steel at 550 and 600°C. Figure 11a shows that at a strain rate of 4×10^{-3} s^{-1}, the curves for thermally aged and sodium-exposed Type 304 stainless steel at 600°C (Fig. 11a) are essentially the same at a total strain range of ∿1.0%. At a lower strain rate of 4×10^{-5} s^{-1}, the curve for the sodium-exposed specimen is higher than that for the aged material which is primarily due to the higher total strain range for the former specimen. The results also show that the material, irrespective of the pretreatment, undergoes significantly more softening at the lower strain rate. The data at 550°C (Fig. 11b) show a large difference in the stress-cycles response between the material in the thermally aged and sodium-exposed conditions. The higher stress associated with the sodium-exposed specimen can be attributed to the higher total strain range and the carburization that occurred during exposure of the specimens to sodium at 550°C. The data for Type 304 stainless steel also show a general trend in which a higher cyclic stress-fatigue cycle response in the material results in a lower fatigue life at a given total strain range (see Figs. 8, 9, and 11a-c).

Figures 11d and 11e show the cyclic stress-fatigue cycle response of Type 316 stainless steel at 600 and 550°C, respectively. The specimens were tested in the annealed, aged, and sodium-exposed conditions at a strain rate of 4×10^{-3} s^{-1} and at a total strain range of ∿1%. The results show that Type 316 stainless steel, in general, strain hardens over a much larger number of fatigue cycles when compared with Type 304 stainless steel. Furthermore, initial strain-hardening rates and the peak stress values are significantly larger in Type 316 than in Type 304 stainless steel. The 550°C test results on Type 316 stainless steel showed secondary hardening after ∿4000 cycles at a strain rate of 4×10^{-3} s^{-1} for different values of total strain range. This phenomenon can be attributed to strengthening of the material by dynamic strain aging at 550°C.

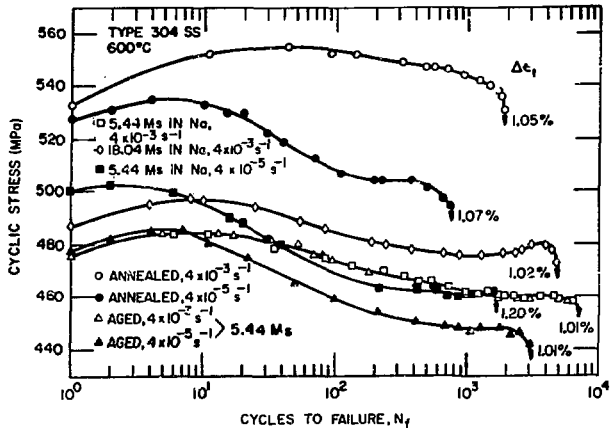

(a)

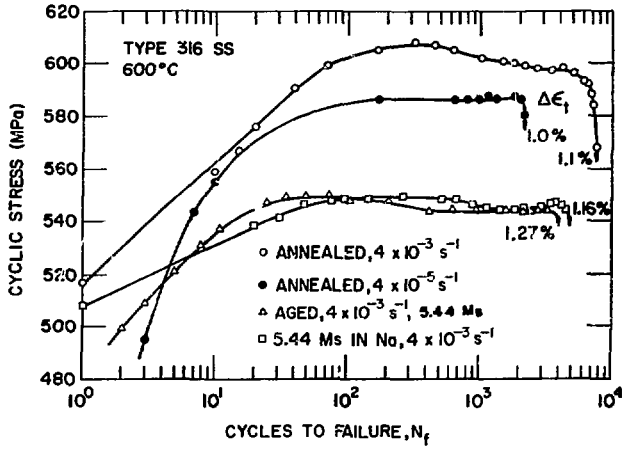

(d)

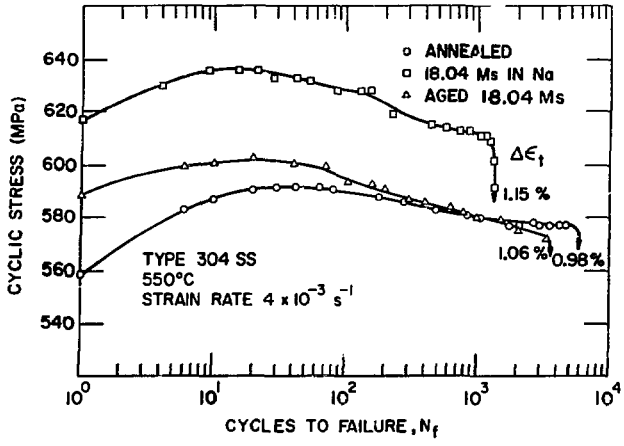

(b)

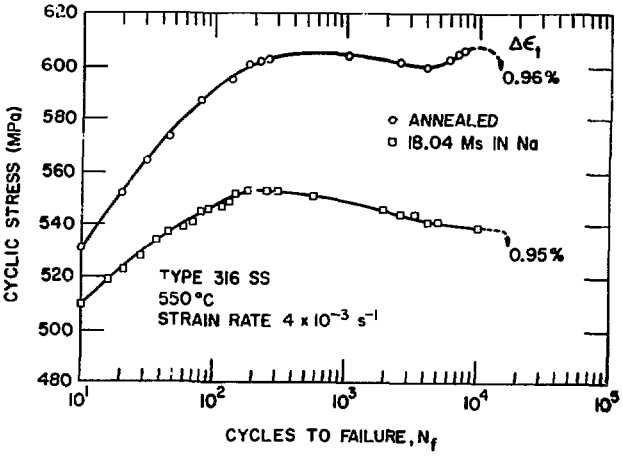

(e)

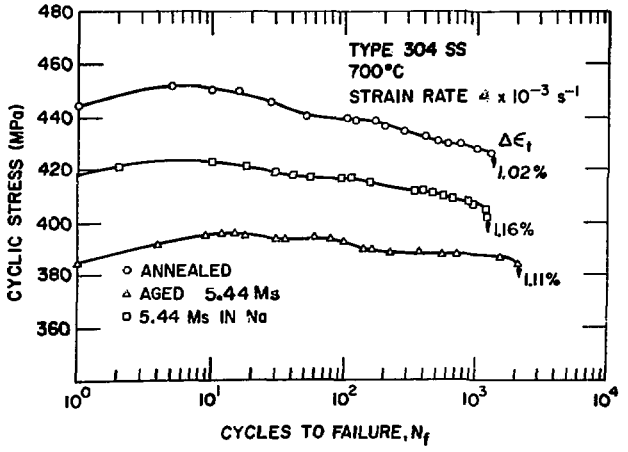

(c)

Fig. 11. Cyclic Stress-fatigue Cycles Response of Type 304 Stainless Steel at (a) 600°C, (b) 550°C, (c) 700°C, and of Type 316 Stainless Steel at (d) 600°C and (e) 550°C.

Microstructural Observations

Optical and scanning-electron microscopy (SEM) were used to examine the cross sections and fracture surfaces of the low-cycle fatigue specimens tested in annealed, aged, and sodium-exposed conditions. Figures 12 and 13 show the optical photographs of cross sections of Types 304 and 316 stainless steel, respectively, in the vicinity of the fracture region. The most striking observation is that the sodium-exposed material, in general, shows a significantly smaller number of cracks when compared with both the annealed and aged materials tested in sodium. For the three material conditions, the cracks were transgranular at a strain rate of 4×10^{-3} s^{-1} and tended toward an intergranular mode at a strain rate of 4×10^{-5} s^{-1}.

Figure 14 shows scanning-electron micrographs of the fracture surfaces of Type 304 stainless steel specimens fatigue tested at a strain rate of 4×10^{-5} s^{-1} at 600°C in the annealed and aged conditions. The low-magnification photographs of the annealed and aged specimens (i.e., center photograph at top and bottom, respectively) show the locations at the surface where the cracks initiated. Figures 14a and 14c are the surface regions of the specimens in higher magnification and show an intergranular mode of crack initiation. The photographs in Figs. 14b and 14d were obtained from the interior regions of the specimens in higher magnification and show the fatigue striations produced during crack propagation.

Figure 15 shows the SEM photographs of the fracture surfaces of Type 304 stainless steel specimens fatigue tested at a strain rate of 4×10^{-3} s^{-1} at 600°C in the annealed, aged, and sodium-exposed conditions. The high-magnification photographs show the fatigue striations that are observed upon testing in a sodium environment. In contrast to the fracture surfaces of specimens tested in air, the striations are not clearly observed in the specimens tested in sodium. However, the fracture surface of annealed material shows intergranular failure and discontinuous striation morphology (Fig. 15b). The aged and sodium-exposed specimens show continuous striations, the width of which increases away from the initiation regions (Figs. 15d and 15f). Considerable uncertainty exists as to whether each striation corresponds to one fatigue cycle for the tests conducted in sodium. Additional information is being developed on the microstructural changes that will be used to examine the roles of crack initiation and propagation in the cyclic fatigue process.

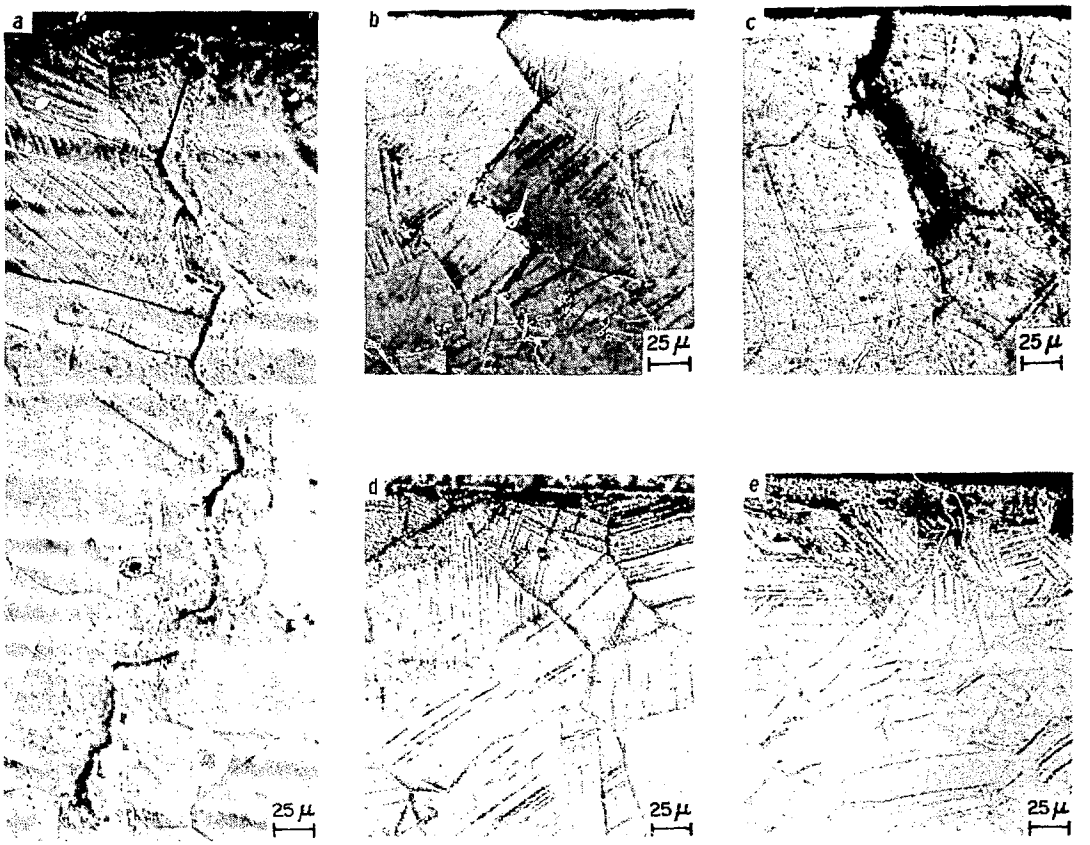

Fig. 12. Optical Photographs of Cross Sections of Type 304 Stainless Steel Fatigue Specimens Tested in Sodium Environment at 600°C. (a) annealed, 4 x 10^{-3} s^{-1}, (b) annealed, 4 x 10^{-5} s^{-1}, (c) aged, 4 x 10^{-3} s^{-1}, (d) 5.44 Ms sodium exposed, 4 x 10^{-3} s^{-1}, and (e) 18.04 Ms sodium exposed, 4 x 10^{-3} s^{-1}.

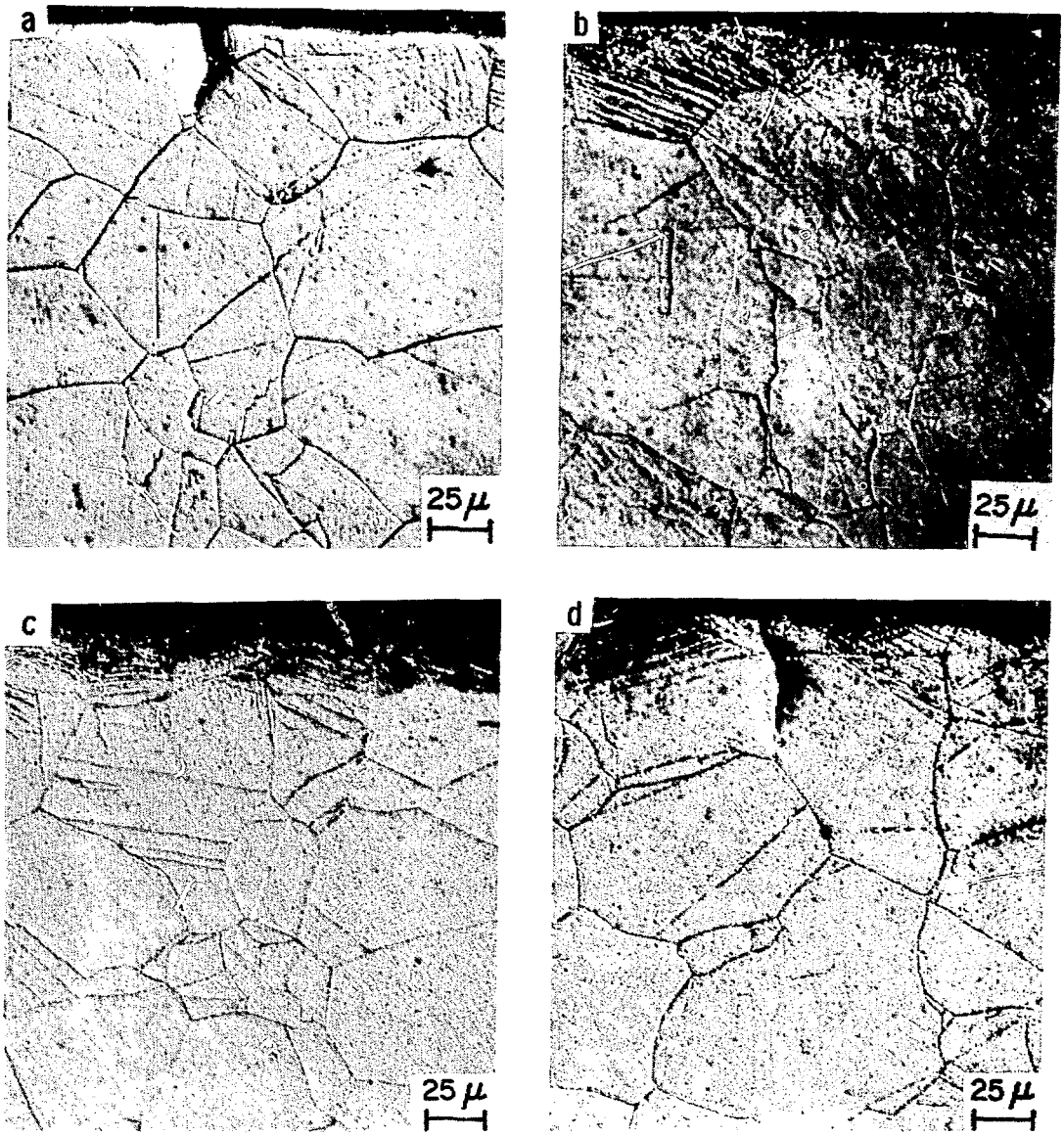

Fig. 13. Optical Photographs of Cross Sections of Type 316 Stainless Steel Fatigue Specimens Tested in Sodium Environment at 600°C. (a) annealed, 4 x 10^{-3} s^{-1}, (b) annealed, 4 x 10^{-5} s^{-1}, (c) aged, 4 x 10^{-3} s^{-1}, and (d) 5.44 Ms sodium exposed, 4 x 10^{-3} s^{-1}.

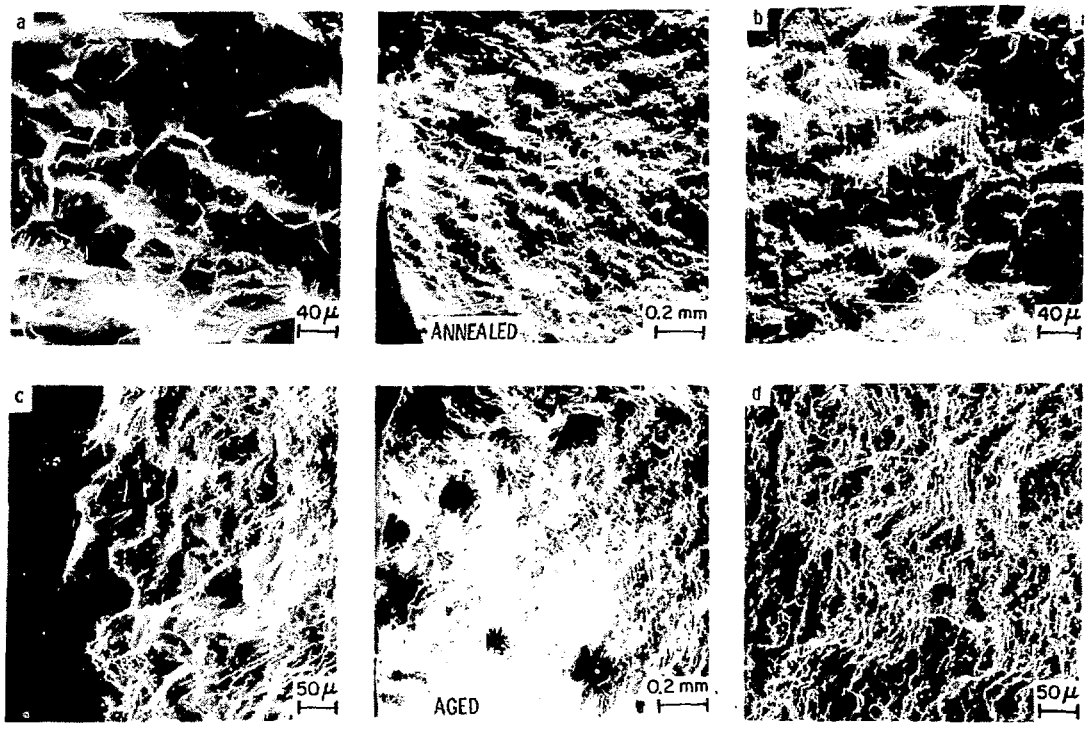

Fig. 14. Scanning-electron Micrographs of Type 304 Stainless Steel Fatigue Specimens Tested at a Strain Rate of 4×10^{-5} s^{-1} at 600°C in the Annealed and Aged Conditions. (a) and (c) crack initiation regions, (b) and (d) crack propagation regions.

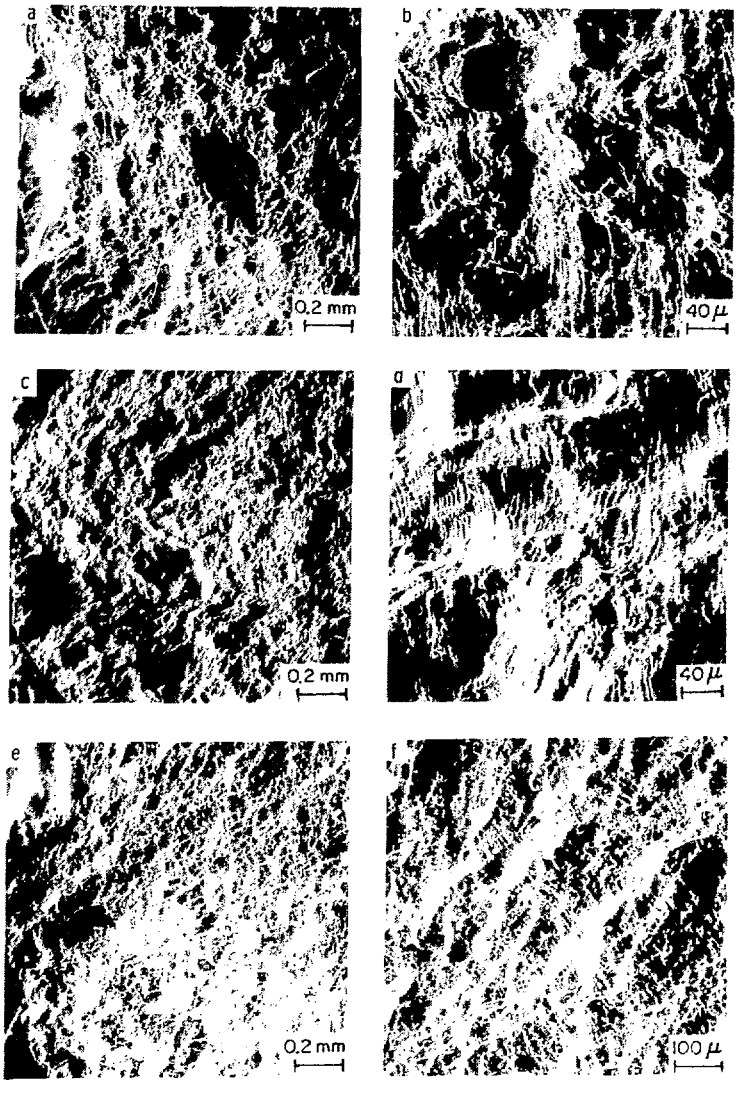

Fig. 15. Scanning-electron Micrographs of Type 304 Stainless Steel Fatigue Specimens Tested at a Strain Rate of 4×10^{-3} s^{-1} at 600°C in Annealed (Top), Aged (Center), and 5.44 Ms Sodium-exposed Conditions (Bottom).

Application of Fatigue Formalisms

A number of phenomenological approaches have been reported in the literature to describe the low-cycle fatigue behavior of a material either with or without the presence of creep damage. Of these, Coffin's[15,16] frequency-modified fatigue-life equations and a damage-rate approach of Majumdar and Maiya[17] are being considered in the creep-fatigue design of structural components. Coffin's method considers the effect of frequency on the fatigue life, whereas the damage-rate approach incorporates the plastic strain rate as a parameter. As a result, the two methods become identical in the life prediction for the case of fully-reversed continuous cycling. For tests that involve hold times at a constant total strain, the stress relaxes and the plastic strain rate decreases continuously during the hold time. Coffin's frequency-modified approach does not consider the deformation and fracture processes when cycles with different wave shapes are applied. As a result, the two methods should differ in the creep-fatigue life prediction under hold-time conditions. The data presented in this paper were generated under fully-reversed cyclic fatigue conditions with no hold time and the information was analyzed by both approaches.

Coffin represented the low-cycle fatigue phenomenon by an empirical formalism

$$N_f^{\alpha} \Delta\varepsilon_p = C, \tag{6}$$

where N_f is the number of cycles to failure, $\Delta\varepsilon_p$ is the plastic strain range, and α and C are parameters. Later the expression was modified to incorporate frequency effects by the relationships

$$C_1^{\beta} \Delta\varepsilon_p = C_2 \tag{7}$$

and

$$C_1 = \nu^k t , \tag{8}$$

where ν is the frequency of the test, t the total time to failure, and C_2 a constant. The parameters β, C_2, and k generally depend on thermal-mechanical history that determines the microstructure of the material. In the solution-annealed specimens, the microstructure changes continuously during the fatigue testing period and the fatigue parameters evaluated from such data would not be appropriate for long-term fatigue life predictions, i.e., for time periods when

most materials attain a metallurgically stable structure. Fatigue data for aged and sodium-exposed Type 304 stainless steel, obtained at strain rates of 4×10^{-3} and 4×10^{-5} s^{-1}, were analyzed to evaluate the parameter k in Eq. (8). Subsequently, a plot of C_1 [calculated from Eq. (8)] versus $\Delta\varepsilon_p$ was constructed and the values for parameters β and C_2 [in Eq. (7)] were computed. The values of different parameters, obtained from the frequency-modified fatigue-life approach, are listed in Table III. Also shown in the table are the constants calculated by Coffin[16] from the experimental data on Type 304 stainless steel obtained by Berling and Slot.[18] The predicted life at 0.2 and 1.0% plastic strain at 600°C based on the present results and from the data of Berling and Slot are also shown in Table III. The difference in the fatigue life from the two sets of data can be attributed to the initial microstructure of the material, since the specimens in Ref. 18 were solution annealed, whereas those of the present work were thermally aged in an argon or sodium environment. At present, a similar analysis cannot be performed for Type 316 stainless steel or for Type 304 stainless steel at other temperatures due to insufficient test data at lower strain rates.

TABLE III. Constants for Fatigue-life Prediction for Type 304 Stainless Steel at 600°C

	k	β	C_2	Predicted Fatigue Life at $\Delta\varepsilon_p$ = 0.2%	Predicted Fatigue Life at $\Delta\varepsilon_p$ = 1.0%
Present work Aged and sodium-exposed material	0.87	0.32	0.106	24450	1600
Coffin's analysis[a] of data from Ref. 18	0.81	0.66	1.0	12280	1070

[a]Interpolated to 600°C.

In the damage-rate approach,[17] it is assumed that the major portion of the life of a low-cycle fatigue specimen is spent in propagation of the preexistent microcracks and that the growth rate of each microcrack (da/dt) can be represented by the equation

$$\frac{da}{dt} = \begin{cases} aT|\varepsilon_p|^m|\dot{\varepsilon}_p|^K & \text{(in the presence of tensile stress)} \\ aC|\varepsilon_p|^m|\dot{\varepsilon}_p|^K & \text{(in the presence of compressive stress)} \end{cases} \tag{9}$$

where a, ε_p, and $\dot{\varepsilon}_p$ are the current microcrack length, plastic strain, and plastic strain rate, respectively, and T, C, m, and K are material parameters that are functions of temperature, environment, and the metallurgical state of the material. For continuous cycling over a plastic strain range $\Delta\varepsilon_p$ at constant plastic strain rate $\dot{\varepsilon}_p$, Eq. (9) has been integrated to give the cycles to failure

$$N_f = \frac{m+1}{4A}\left(\frac{\Delta\varepsilon_p}{2}\right)^{-(m+1)}(\dot{\varepsilon}_p)^{1-K}, \tag{10}$$

where $A = \frac{C+T}{2}\Big/\ln\frac{a_c}{a_o}$, and a_o, a_c are the initial and final crack lengths.

The fatigue data on annealed, aged, and sodium-exposed materials were used in Eq. (10) to obtain the parameters m, K, and A. The calculated values are given in Table IV. The results show that at a temperature of 600°C, the material condition has significant effect on m, i.e., the slope of the plastic strain range versus fatigue life curve. The increase in m value from 1.28 to 2.74 as the strain rate decreases from 4×10^{-3} to 4×10^{-5} s^{-1} results from the longer test duration at lower strain rate, which produces additional thermal aging of the material. Similar values for the annealed material at low strain rate and for the aged and sodium-exposed specimens also confirm the aging effect.

The values for the parameter A obtained from the present work are 1.2×10^2 and 3.8×10^5 for the annealed material tested at strain rates of 4×10^{-3} and 4×10^{-5} s^{-1}, respectively. These values are considerably greater than the reported[17] values of 1 to 8 for Type 304 stainless steel tested at similar plastic strain rates in an air environment. The calculations show that at all the temperatures of the present investigation, thermal aging or sodium exposure of Type 304 stainless steel increases the m values and improves the endurance life (the fatigue life at $N_f > 10^6$) when compared with solution-annealed material. The values of parameter K, which reflect the effect of strain rate on the fatigue life, are 0.94 and 0.86 for Type 304 stainless steel in the annealed condition and after aging in an argon or sodium environment, respectively. The influence of strain rate on the fatigue life in the present work is quite small, since K = 1.0 indicates no strain-rate effect.

TABLE IV. Damage-rate Equation Coefficients Calculated from Fatigue Data for Types 304 and 316 Stainless Steel

Temperature, °C	Strain Rate, s^{-1}	Material Condition	m	K	A
		Type 304 Stainless Steel			
600	4×10^{-3}	Annealed	1.28	0.94	1.2×10^{2}
		Aged and Na exposed	2.26	0.86	9.6×10^{3}
	4×10^{-5}	Annealed	2.74	0.94	3.8×10^{5}
		Aged and Na exposed	2.19	0.86	6.6×10^{3}
550	4×10^{-3}	Annealed	1.10		
		Aged	1.73		
		Na exposed	2.40		
700	4×10^{-3}	Annealed	1.09		
		Aged	1.76		
		Na exposed	1.65		
		Type 316 Stainless Steel			
600	4×10^{-3}	Annealed	1.97		
		Aged and Na exposed	2.25		
550	4×10^{-3}	Annealed and Na exposed	0.81		
700	4×10^{-3}	Annealed and Na exposed	1.79		

The fatigue data for Type 316 stainless steel at 600°C show almost no variation in the m value with material condition. Additional data on Type 316 stainless steel are required at low strain rates to evaluate the parameters and to apply the damage-rate equations for fatigue life predictions.

SUMMARY

Uniaxial creep-rupture and low-cycle fatigue data were obtained for Types 304 and 316 stainless steel in solution-annealed, thermally aged, and sodium-exposed conditions at temperatures between 550 and 700°C. A carbon concentration of ∿0.4 ppm in sodium, which is a factor of two larger than in EBR-II primary sodium circuit, was selected for the exposure of the mechanical test specimens. The creep behavior of the steels carburized in a sodium environment showed an increase in rupture life and a decrease in minimum creep rate (except for Type 316 stainless steel at 550°C) when compared with annealed material at temperatures between 550 and 700°C. Microstructural examination of creep-tested specimens showed that sodium exposure inhibited intergranular failure that is generally observed at lower strain rates. The experimental data were used to develop creep correlations that aid in the evaluation of creep quantities, such as minimum creep rate and time-to-tertiary creep, from standard stress-rupture tests. Isochronous stress-creep strain curves were generated for the steels in both the solution-annealed and sodium-exposed conditions, with the use of a single polynomial creep equation.

The low-cycle fatigue data obtained at 600°C on annealed, aged, and sodium-exposed specimens of Types 304 and 316 stainless steel showed that thermal aging of the materials in either argon or sodium had a significant effect on fatigue life. The data at 550°C on sodium-exposed specimens, which had a surface carbon content of ∿0.8 wt %, showed a lower fatigue life when compared with that of the aged material. In general, a decrease in strain rate by two orders of magnitude reduced the fatigue life by a factor of two at 600°C. Results on the cyclic stress-fatigue life response indicated a greater strain-hardening rate for Type 316 than for Type 304 stainless steel under all material conditions. Microstructural examination of the fatigue specimens showed a significantly smaller number of cracks after sodium exposure than in the annealed condition. The cracks observed were transgranular at a strain rate of 4×10^{-3} s^{-1} and tended toward an intergranular mode at a strain rate of 4×10^{-5} s^{-1}.

The fatigue results were analyzed using Coffin's frequency-modified fatigue-life equations and a damage-rate approach developed at ANL. The calculations showed that the initial microstructure of the material had a strong influence on the β and C_2 parameters, which in turn had an effect on the fatigue-life predictions. The experimental data and calculated fatigue-life predictions indicated that thermal aging and sodium exposure of Type 304 stainless steel increased the endurance life when compared with material in the annealed condition. Based on the results described in the present work and on the expected carbon concentrations in LMFBR primary system sodium, moderate carburization of the austenitic stainless steels will not degrade the mechanical properties to a significant extent, and therefore, will not limit the performance of out-of-core components.

ACKNOWLEDGMENTS

The authors gratefully acknowledge the assistance of D. L. Rink, R. R. Schlueter, S. Mihailovich, J. A. Lahti, and R. W. Bunce in performing the specimen exposures to sodium and the creep-rupture tests, R. H. Lee and J. F. Arko in conducting low-cycle fatigue tests in a sodium environment, and S. M. Hagamann for typing the manuscript. This work was supported by the U. S. Energy Research and Development Administration.

REFERENCES

1. K. Natesan, T. F. Kassner, and Che-Yu Li, "Effect of Sodium on the Mechanical Properties and Friction-Wear Behavior of LMFBR Materials," *Reactor Technology* 15, 244 (1972-1973).

2. R. B. Snyder, K. Natesan, and T. F. Kassner, "An Analysis of Carbon Transport in the EBR-II and FFTF Primary Sodium Systems," *Proceedings of the Intl. Conf. on Liquid Metal Technology in Energy Production,* CONF-760503-P2, Paper VIII B-3, p. 826 (1976).

3. R. B. Snyder, K. Natesan, and T. F. Kassner, "Kinetics of the Carburization-Decarburization Process of Austenitic Stainless Steels in Sodium," *J. of Nucl. Mater.* 50, 259 (1974).

4. D. L. Smith, K. Natesan, T. F. Kassner, and G. J. Zeman, "Effects of Sodium on the Low-cycle Fatigue Behavior of Austenitic Stainless Steels," *ASME Symposium on Structural Materials for Service at Elevated Temperatures in Nuclear Power Generation,* MPC-1, p. 290 (1975).

5. K. Natesan, D. L. Smith, T. F. Kassner, and O. K. Chopra, "Influence of Sodium Environment on the Tensile Behavior of Austenitic Stainless Steels," ibid, p. 302 (1975).

6. K. Natesan and T. F. Kassner, "Monitoring and Measurement of Carbon Activity in Sodium Systems," *Nuclear Technology* 19, 46 (1973).

7. K. Natesan, O. K. Chopra, and T. F. Kassner, "Effect of Sodium Environment on the Creep-rupture Behavior of Austenitic Stainless Steel," to be publisted in the *Proceedings of the Fifth Intl. Symp. on Heat-Resistant Metal Materials*, Vsetin, Czechoslovakia, September 1976.

8. O. K. Chopra and K. Natesan, "Representation of Elevated Temperature Tensile Behavior of Type 304 Stainless Steel in a Sodium Environment," to be published in the *J. of Engr. Mater. and Technology*, ASME.

9. K. Natesan, O. K. Chopra, and T. F. Kassner, "Effect of Sodium on the Creep-rupture Behavior of Type 304 Stainless Steel," *Proceedings of the Intl. Conf. on Liquid Metal Technology in Energy Production*, CONF-760503-P1, Paper VA-4, p. 338 (1976).

10. Interpretations of the ASME Boiler and Pressure Vessel Code, Case 1592, American Society of Mechanical Engineers (1974).

11. L. D. Blackburn, J. C. Tobin, and R. A. Moen, "Materials Creep Behavior and Elevated Temperature Design," *Nuclear Technology* 16, 278 (1972).

12. M. K. Booker, Oak Ridge National Laboratory, private communication.

13. D. L. Smith, G. J. Zeman, K. Natesan, and T. F. Kassner, "Influence of Sodium on the Low-cycle Fatigue Behavior of Types 304 and 316 Stainless Steel," *Proceedings of the Intl. Conf. on Liquid Metal Technology in Energy Production*, CONF-760503-P1, Paper VA-7, p. 359 (1976).

14. G. J. Zeman and D. L. Smith, "Low-cycle Fatigue Behavior of Types 304 and 316 Stainless Steel Tested in Sodium at 550°C," to be published.

15. L. F. Coffin, "Predictive Parameters and Their Application to High Temperature, Low-cycle Fatigue," in *Fracture* 1969 (Proc. Second Intl. Conf. on Fracture), Chapman and Hall, London, p. 643 (1969).

16. L. F. Coffin, "The Effect of Frequency on the Cyclic Strain and Low-cycle Fatigue Behavior of Cast Udimet 500 at Elevated Temperature," *Met. Trans.* 2, 3105 (1971).

17. S. Majumdar and P. S. Maiya, "A Unified and Mechanistic Approach to Creep-fatigue Damage," Argonne National Laboratory, ANL-76-58 (1976).

18. J. T. Berling and T. Slot, "Effect of Temperature and Strain Rate on Low-cycle Fatigue Resistance of AISI 304, 316, and 348 Stainless Steels," *ASTM Symp. on Fatigue at High Temperature*, ASTM-STP 459, p. 3 (1969).